Electronic Supplementary Material (ESI) for Journal of Materials Chemistry A.

Interface regulation using a fluorinated vinylene-linked covalent organic framework for a highly stable Zn anode

Yanjie Wang,[a] Ning Li,[a] Huiyan Liu,[a] Haoyang Sun,[a] Zhuo Wang,[a] Lipeng Zhai,*[a] Kongyao Chen,[a] Liwei Mi,*[a,b] Zhe Fang[a] and Yunhui Huang *[c]

[a] Henan Key Laboratory of Functional Salt Materials, Center for Advanced Materials Research, Zhongyuan University of Technology, Zhengzhou 450007, P. R. China

E-mail: zhailp@zut.edu.cn, mlwzzu@163.com

[b] Yaoshan laboratory, Pingdingshan University, Pingdingshan Henan 467000, P. R. China

[c] State Key Laboratory of Material Processing and Die & Mould Technology, School of Materials Science and Engineering, Huazhong University of Science and Technology, Wuhan 430074, P. R. China

E-mail: huangyh@hust.edu.cn

Experimental Section

All chemicals used in this study were purchased from Sinopharm Chemical Reagent Co., Ltd., Beijing Innochem Science & Technology Co., Ltd., or Shanghai Aladdin Biochemical Technology Co., Ltd. These chemicals are of analytical grade and used without further purification.

Material preparation.

Synthesis of TM-TA-COF. A Pyrex tube (10 mL) was charged with 2,4,6-trimethyl-1,3,5-triazine (0.25 mmol), terepthalaldehyde (TA, 0.375 mmol), KOH (42.0 mg, 0.75 mmol), 3.5 mL n-Butanol and 1.5 mL 1,2-dichlorobenzene. Subsequently, the resulting pale-yellow solution was heated at 120 ℃ for 3 days. After cooling to room temperature, the precipitate was collected and washed with methanol, tetrahydrofuran, acetone and dichloromethane in sequence for three times, and then dried under vacuum at 120 °C for overnight. Finally, pure COF sample was afforded as yellow powder with 80% yield.

Synthesis of TM-4F-COF. A Pyrex tube (10 mL) was charged with 2,4,6- trimethyl-1,3,5-triazine (TM, 0.1 mmol), 2,3,5,6-tetrafluoroterephthalaldehyde (4F, 0.15 mmol), 0.9 mL mesitylene, 0.9 mL 1,4-dioxane, 0.40 mL trifluoroacetic acid, and 50 μL acetonitrile. The tube was then flash frozen at 77 K and degassed by three freeze-pump-thaw cycles. The tube was sealed and heated at 150 °C for 3 days. The collected powder was neutralized by 0.1 mol L-1 NH_4OH solution in aqueous methanol (50 wt%) and washed with THF and methanol for two times. The solid was then washed with methanol in a Soxhlet extractor for another 12 h. Subsequently, the product was dried at 120 °C under vacuum for 12 h to obtain the corresponding yellow powder in ~78% isolated yield.

Material characterizations. The morphology and element composition of samples are carried out on scanning electron microscope (SEM, Zeiss Merlin Compact, Germany) equipped with energy dispersive spectroscopy (EDS). X-ray diffraction (XRD) (Rigaku Ultima IV, Japan) and X-ray photoelectron spectroscopy (XPS, Thermo ESCALAB 250XIy) are used to analyse the phase and element state of samples. The Fourier Transform Infrared Spectroscopy (FTIR) is measured on Perkin Elmer Frontier. And Brunauer-Emmett-Teller (BET) specific surface area of TM-4F-COF and TM-TA-COF are obtained via nitrogen adsorption at 77 K on an ASAP-2010 analysis system (Micro meritics, U.S.A.). Thermogravimetric analysis (TGA) was obtained using a Mettler-Toledo model TGA/SDTA851e under N_2 by heating the sample to 800 °C at a rate of 10 °C min^{-1}.

Electrochemical device assembly

The preparation process of TM-4F-COF@Zn and TM-TA-COF@Zn electrode sheet. Mixing the TM-4F-COF powder and PVDF (the weight ratio is 9:1) into appropriate NMP solvent to obtain homogeneous sizing agent. Then above homogeneous sizing agent are uniformly coated on Zn foil to obtain TM-4F-COF@Zn electrode. The preparation process of TM-TA-COF@Zn electrode was similar with TM-4F-COF@Zn electrode.

Assembly of Zn//Zn symmetric cell. The CR2032 coin type Zn//Zn symmetric cell was assembled by choosing two same pure Zn sheets with a diameter of 8 mm as electrodes, 2 M $ZnSO_4$ as electrolyte and glass fiber as separator. The assembly process of TM-4F-COF@Zn//TM-4F-COF@Zn or TM-TA-COF@Zn//TM-TA-COF@Zn was similar to that of Zn//Zn symmetric cell.

Assembly of Zn//Ti half cell. The CR2032 coin type Zn//Ti half cell was assembled using Ti foil as working electrode and pure Zn as counter electrode, selecting 2 M $ZnSO_4$ as electrolyte and glass fiber as separator. The assembly process of TM-4F-COF@Zn//Ti or TM-TA-COF@Zn//Ti was similar to that of pure Zn//Ti half cell.

Preparation of V_2O_5. NH_4VO_3 (0.648 g) was dissolved into 90 mL H_2O, and then 2 mL 1 mol L^{-1} HCl was added in above solution drop by drop. After stirred for 10 min, 6 mL of $N_2H_4 \cdot H_2O$ (80%) was added drop by drop. After reaction at 140 ^oC for 6 h, the powder was obtained by centrifugation and dried overnight. Finally, V_2O_5 can be obtained after calcined at 400 ^oC for 2 h.

Assembly of Zn//V_2O_5 batteries and Zn//AC capacitors. First, the V_2O_5 electrode is prepared through coating the mixed slurry of V_2O_5 power, acetylene black, PVDF (the mass ratio is 7:2:1) in NMP solution on Ti foil. The Ti foil was following cut into circular electrode piece with the diameter of 0.8 mm. The average mass loading of active material was about to be 1 mg cm^{-2}. Choosing V_2O_5 electrode sheet as cathode, pure Zn or TM-4F-COF@Zn or TM-TA-COF@Zn sheet as anode, 2 M $ZnSO_4$ as electrolyte, glass fiber as separator, the CR2032 coin type Zn//V_2O_5, TM-TA-COF@Zn//V_2O_5 and TM-TA-COF@Zn//V_2O_5 batteries were assembled. According to the similar assembly process with Zn//V_2O_5 batteries, Zn//activated carbon (Zn//AC) capacitors can be fabricated by choosing AC as cathode**.**

In situ observation process of transparent Zn-based symmetrical cells. Firstly, two Zn sheets were placed in a transparent cuvette filled with 2 M $ZnSO_4$ electrolyte. Then, Zn

plating/stripping process, performed on a CHI660E electrochemical workstation, was observed *in situ* through an optical microscope.

Electrochemical measurements. All the cyclic voltammetry (CV) curves and impedance spectroscopy (EIS) are measured on an electrochemical workstation (Chenhua CHI 660e, Shanghai). And the Zn plating/stripping curves are obtained on a battery testing system (LAND CT 2001A, Wuhan). The frequency range of EIS is from 100 kHz to 0.01 Hz with an alternating voltage amplitude of 5 mV. Linear sweep voltammetry (LSV) curves were obtained using a three-electrode system with Zn or TM-4F-COF@Zn as the working electrode, Pt as the counter electrode, and Ag/AgCl as the reference electrode in 1 M $NaSO_4$ solution. Linear polarization curves were tested at a scan rate of 1 mV s^{-1} between -0.85 and -1.1 V (with respect to the Ag/AgCl electrode).

Computational calculations. The computational calculation for the distribution of electric field and Zn^{2+} concentration. FEM conducted by COMSOL Multiphysics has been used to investigate the distribution of Zn ions through our structure. The migration of Zn ions driven by electric field and diffusion flow in both liquid phase (electrolytes) and solid phase was taken into account in these simplified simulations. Two physical models of electrostatic and transport of diluted species based on the partial differential equations listed below were coupled to conduct FEM simulation[1].

$$E = -\nabla\phi$$
$$N = -D\nabla = c + ucE$$

$$\frac{\partial \mathrm{c}}{\partial \mathrm{t}} = -\nabla \mathrm{N}$$

where ϕ is the electric potential, E is the electric field, D is the diffusion coefficient of Zn ions, c is the concentration of Zn ions, u is the ionic mobility of Zn ion in electrolytes, and N is the flux vector of Zn ions, t is the diffusion time. These FEM simulations on the routine our composite separator was performed in a rectangle area, respectively. The potential difference $\Delta\phi$ through these electrolytes was set as 50 mV. To investigate the ion transport behaviors with limited liquid electrolytes in long time cycling, the same physical model was established and the ratio of diffusion coefficients of Zn ions in liquid electrolytes and solid particles was decreased to 10.0. The mobilities of Zn ions m for liquid electrolyte and solid particles are defined by the Nernst-Einstein equation. The bottom boundaries of two simulation areas are the Dirichlet boundaries with $\phi_0 = 0$ V and $c_0 = 0$ M. The top boundaries of two simulation area are also Dirichlet boundaries with $\phi 1 = 25$ mV and c1 = 1.2 M. The other boundaries are natural boundaries with zero flux.

The computational calculation for Zn(002) surface energy and desolvation energy. The Vienna Ab Initio Package (VASP) was employed to perform all the density functional theory (DFT) calculations within the generalized gradient approximation (GGA) using the Perdew, Burke, and Enzerhof (PBE) formulation. [2–4]The projected augmented wave (PAW) potentials were applied to describe the ionic cores and take valence electrons into account using a plane wave basis set with a kinetic energy cutoff of 450 eV. [5,6]Partial occupancies of the Kohn–Sham orbitals were allowed using the Gaussian smearing method and a width of 0.05 eV. The electronic energy was considered self-consistent when the energy change was smaller than 10^{-4}eV. A geometry optimization was considered convergent when the force change was smaller than 0.03 eV/Å. Grimme's DFT-D3 methodology was used to describe the dispersion interactions. The equilibrium lattice constants unit cell was optimized when using a 2× 2× 1Monkhorst-Pack k-point grid for Brillouin zone sampling. The surface energies were calculated by dividing the difference between the energy of our slabs and the same amount of units in the bulk by the surface area of the slab including both sides of the slab:

$$E_{surface} = \frac{E_S}{2S} - \frac{nE_b}{2S}$$

Here, Eb is the total energy per formula unit of bulk, Es is the total energy of the given supercell containing n formula units of Zn, S is the base area of the supercell. The vacuum spacing perpendicular to the plane of the structure is 10 Å. The Brillouin zone integral utilized the surfaces structures of 3 × 3 × 1 monkhorst pack K point sampling. The desolvation energy is calculated.

The computational calculation for the free energy of electrochemical hydrogen evolution (HER) process[2,4,5,7]. We have employed the first-principles to perform all Spin-polarization density functional theory (DFT) calculations within the generalized gradient approximation (GGA) using the Perdew-Burke-Ernzerhof (PBE) formulation. We have chosen the projected augmented wave (PAW) potentials to describe the ionic cores and take valence electrons into account using a plane wave basis set with a kinetic energy cutoff of 450 eV. Partial occupancies of the Kohn−Sham orbitals were allowed using the Gaussian smearing method and a width of 0.05 eV. The electronic energy was considered self-consistent when the energy change was smaller than 10^{-5} eV. A geometry optimization was considered convergent when the energy change was smaller than 0.03 eV $Å^{-1}$. The vacuum spacing in a direction perpendicular to the plane of the structure is 20 Å for the Zn surfaces. The Brillouin zone integration is performed using 3×3×1 Monkhorst-Pack k-point sampling for a structure. Finally, the adsorption energies (Eads) were calculated as Eads= Ead/sub -Ead -Esub, where Ead/sub, Ead, and Esub are the

total energies of the optimized adsorbate/substrate system, the adsorbate in the structure, and the clean substrate, respectively. The free energy was calculated using the equation:

$$G=Eads+ZPE-TS$$

where G, Eads, ZPE and TS are the free energy, total energy from DFT calculations, zero-point energy and entropic contributions, respectively.

Supporting Figures

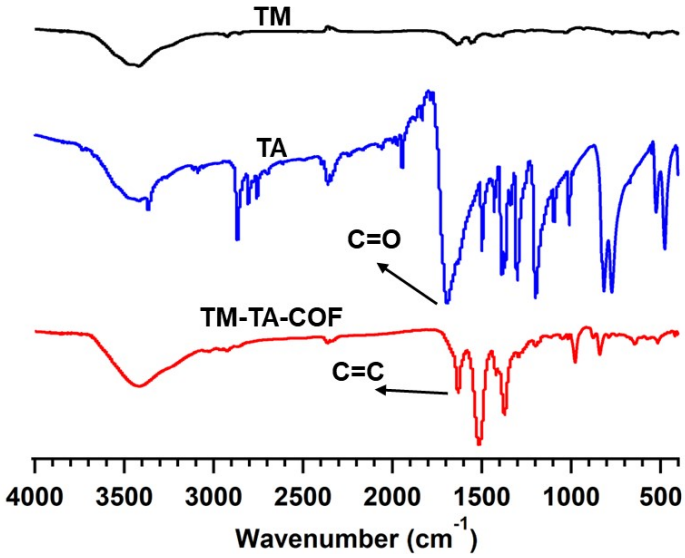

Figure S1. FT-IR spectra of TM-TA-COF.

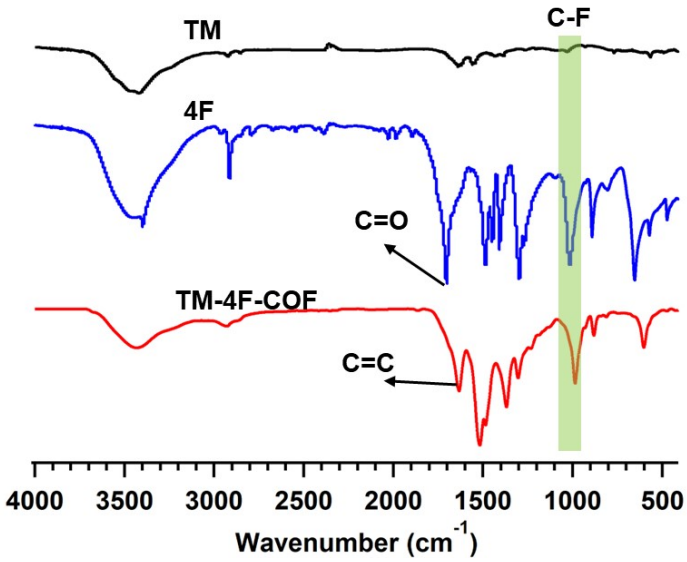

Figure S2. FT-IR spectra of TM-4F-COF.

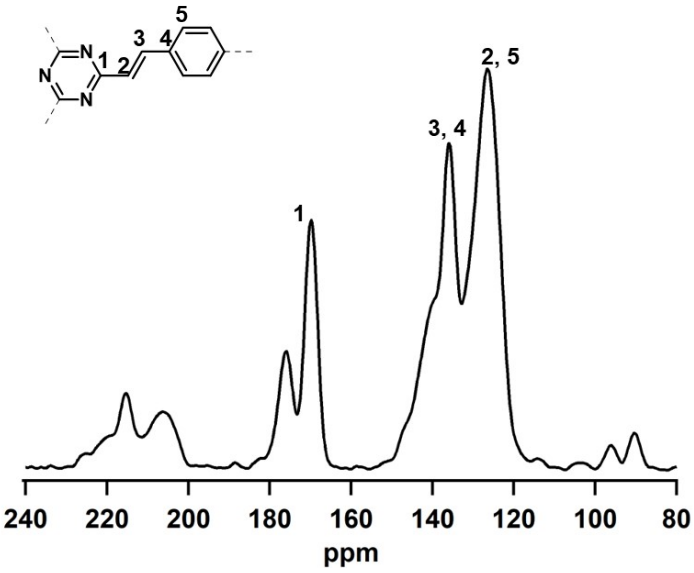

Figure S3. The NMR result of TM-TA-COF.

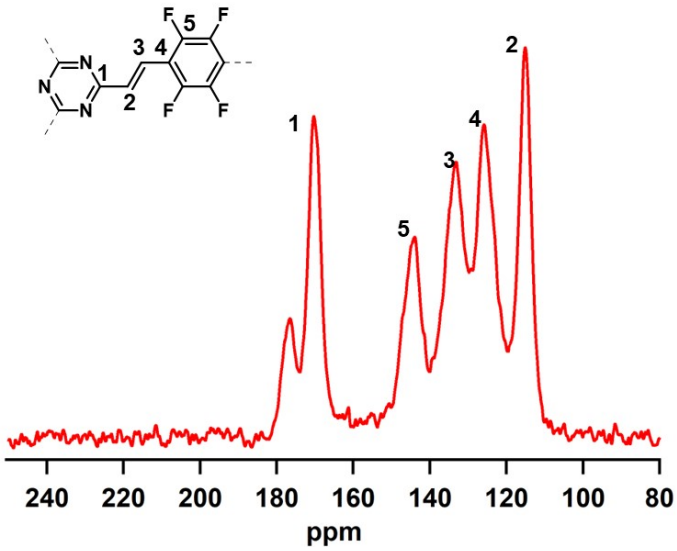

Figure S4. The NMR result of TM-4F-COF.

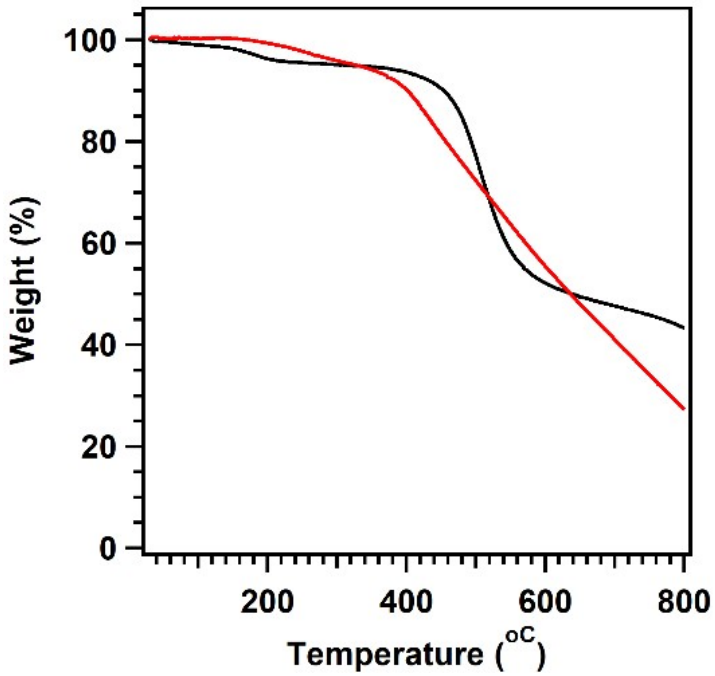

Figure S5. The TG curves of TM-TA-COF (black) and TM-4F-COF (red).

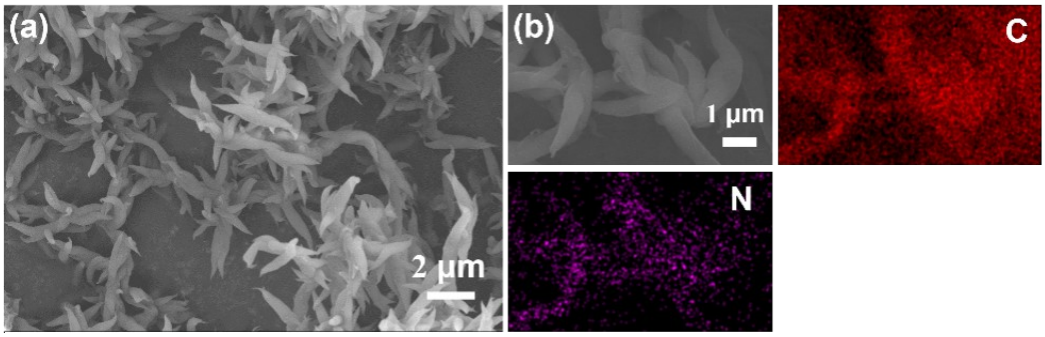

Figure S6. The SEM image (a) and EDS mapping (b) of C and N element of TM-TA-COF.

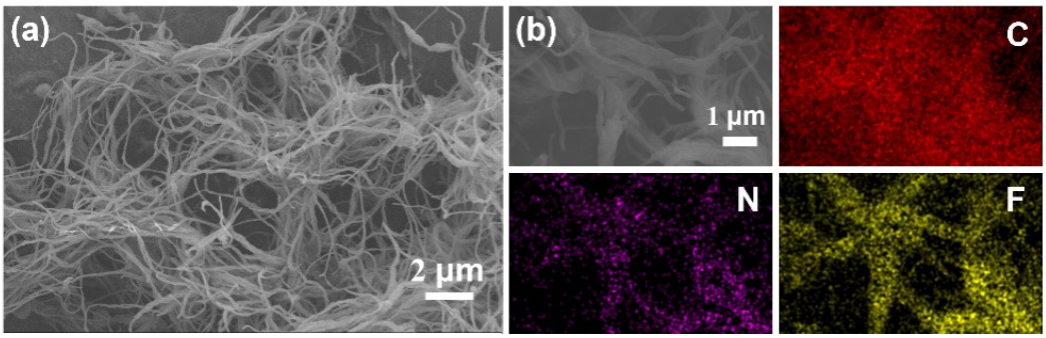

Figure S7. The SEM image (a) and EDS mapping (b) of C and N element of TM-4F-COF.

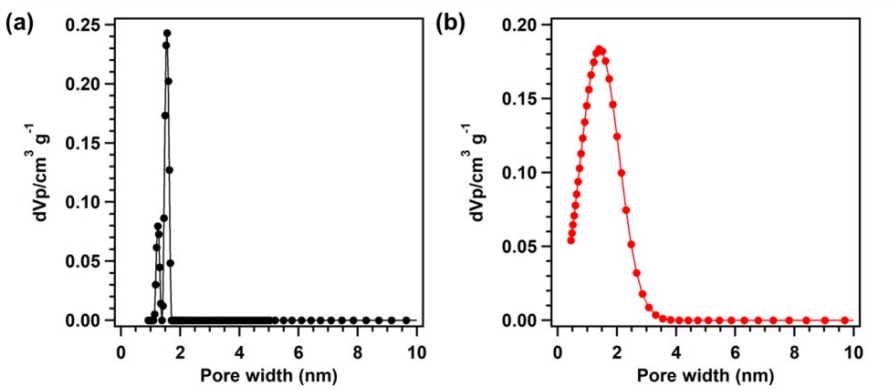

Figure S8. The pore size distribution profiles of TM-TA-COF (a) and TM-4F-COF (b).

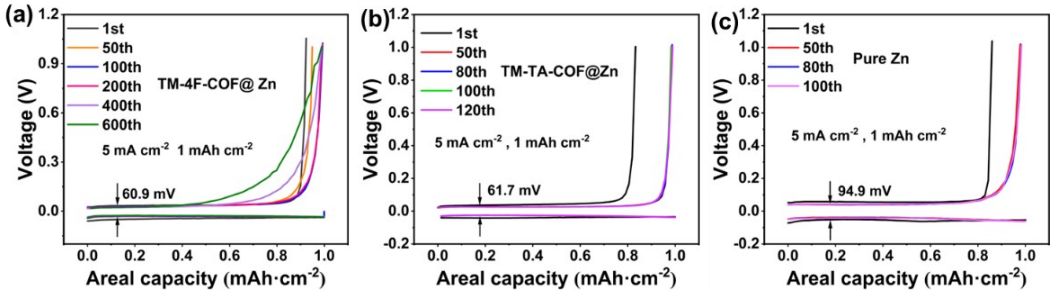

Figure S9. The Zn plating/stripping curves of TM-4F-COF@Zn//Ti (a), TM-TA-COF@Zn//Ti (b) and pure Zn//Ti (c) half cells.

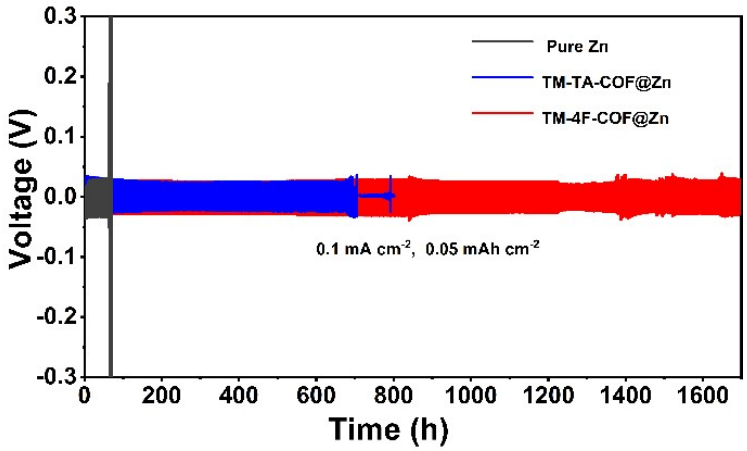

Figure S10. The Zn plating/stripping curves of Zn-based symmetrical cells at 0.1 mA cm^{-2}, 0.05 m Ah cm^{-2}.

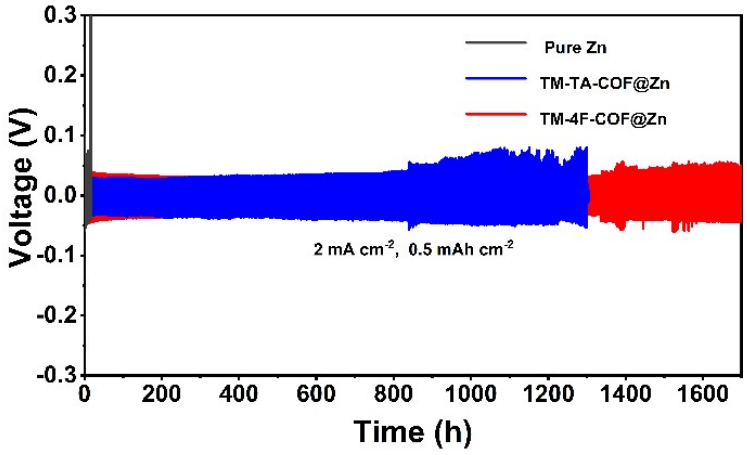

Figure S11. The Zn plating/stripping curves of Zn-based symmetrical cells at 2 mA cm^{-2}, 0.05 m Ah cm^{-2}.

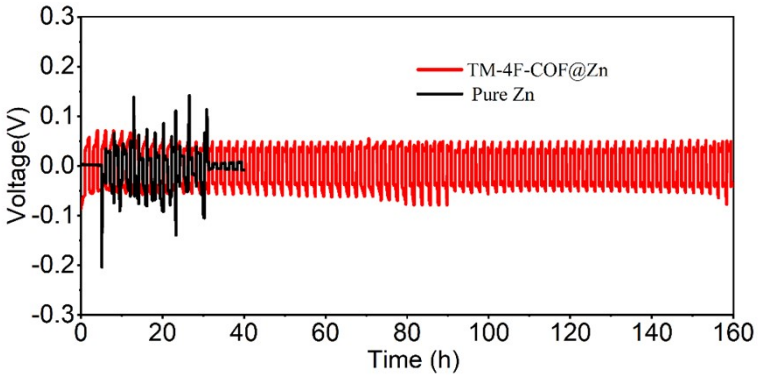

Figure S12. The Zn plating/stripping curves of Zn-based symmetrical cells at 5 mA cm^{-2}, 5 m Ah cm^{-2}.

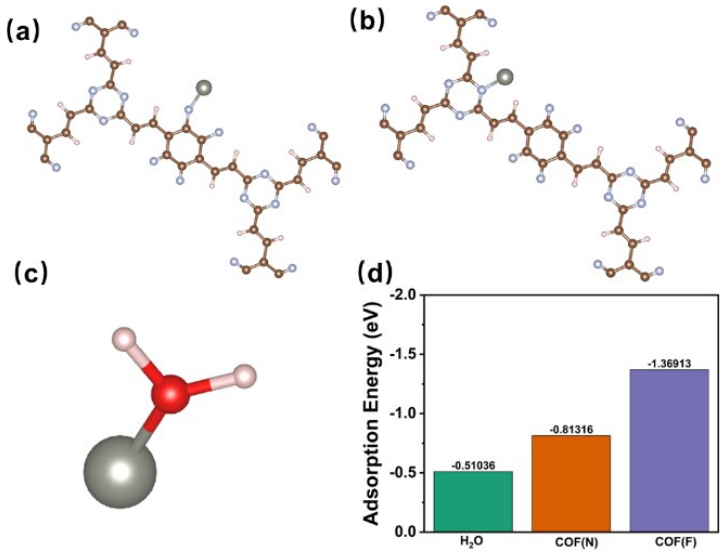

Figure S13. (a-c) The molecular model of adsorption site of Zn-TM-4F-COF(F) (site1, COF(F)) (a)， Zn-TM-4F-COF(N) (site 2, COF(N)) (b) and Zn-H_2O (site 3, c). (d) the calculated adsorption energy of TM-4F-

COF(F), TM-4F-COF(N) and Zn-H_2O with Zn^{2+}.

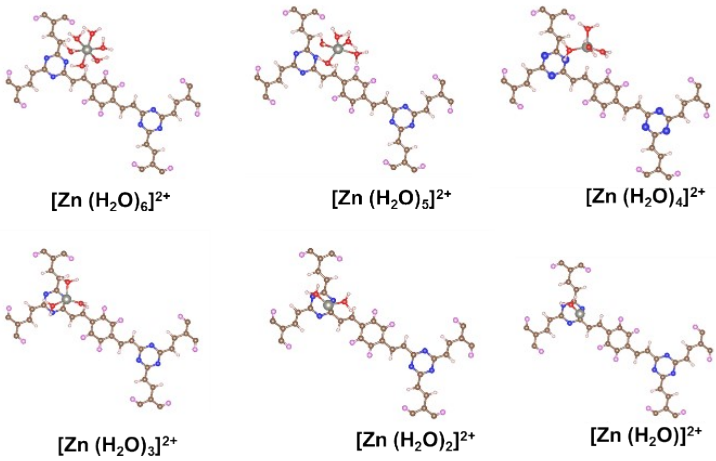

Figure S14. The forms of hydrated Zn^{2+} ($[Zn(H_2O)_6]^{2+}$) at TM-4F-COF.

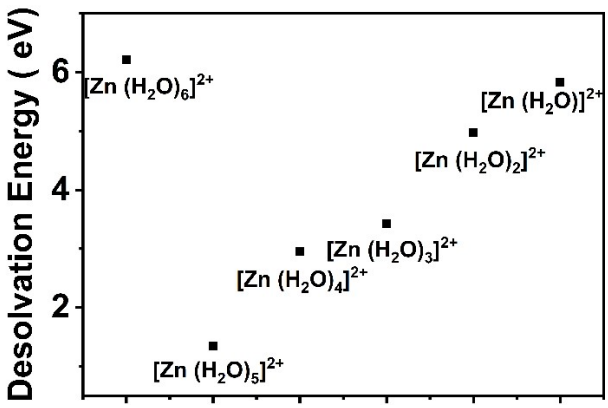

Figure S15. The desolvation energy of various hydrated Zn^{2+} at TM-4F-COF.

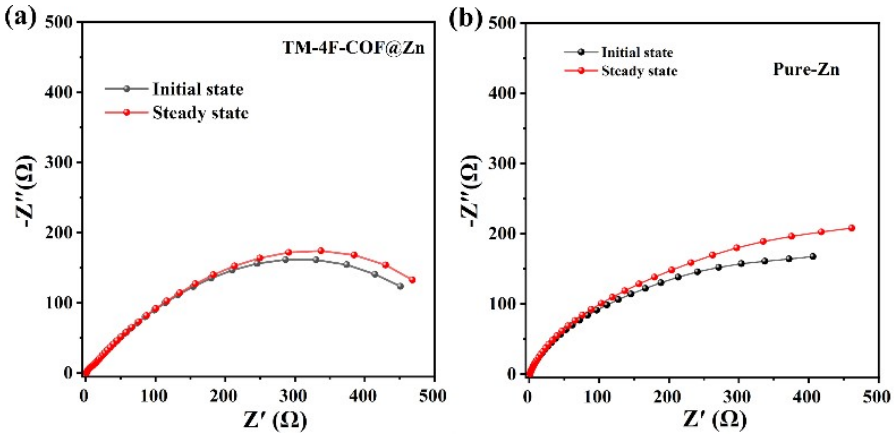

Figure S16. The initial-state and steady-state electrochemical impedance spectroscopy (EIS) spectra of TM-4F-COF@Zn (a) and pure Zn (b).

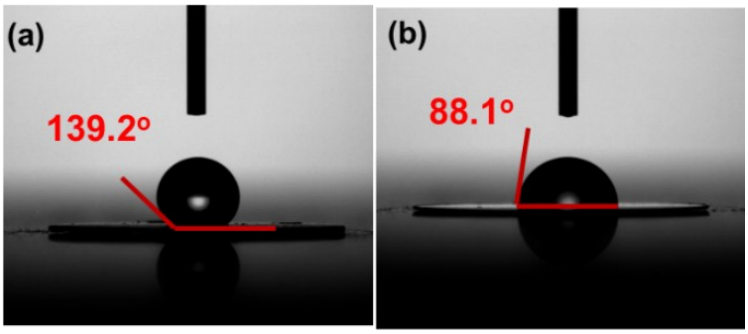

Figure S17. The contact angle of H_2O on TM-4F-COF@Zn (a) and pure Zn (b).

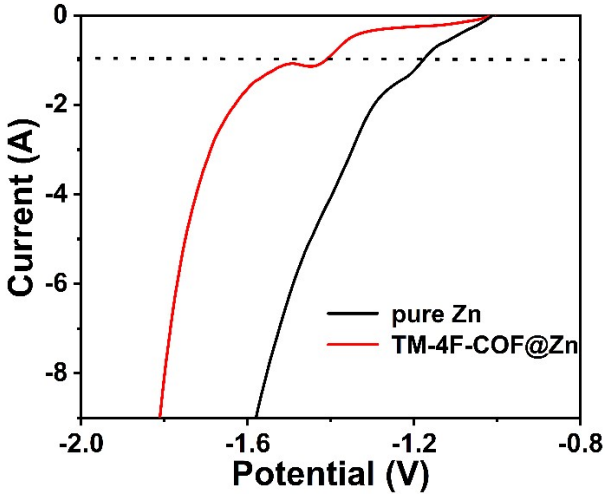

Figure S18. The linear sweep voltammetry (LSV) curves of TM-4F-COF@Zn and pure Zn in Na_2SO_4.

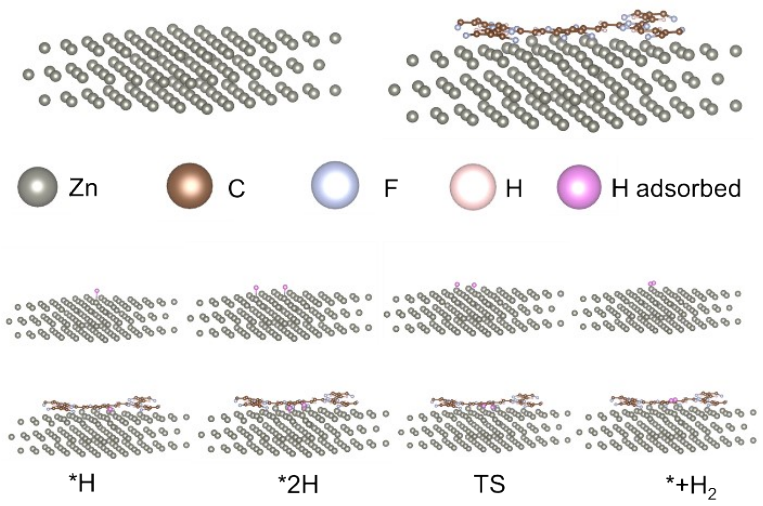

Figure S19. Computational models for the theoretical calculation of electrochemical hydrogen evolution reactions (HER) process.

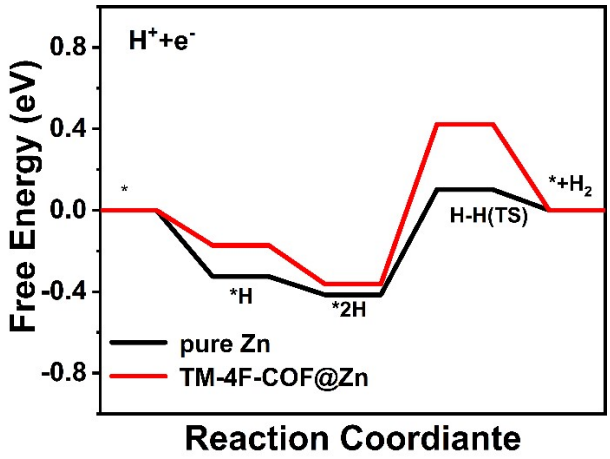

Figure S20. The calculated free energy for electrochemical hydrogen evolution reactions (HER) process.

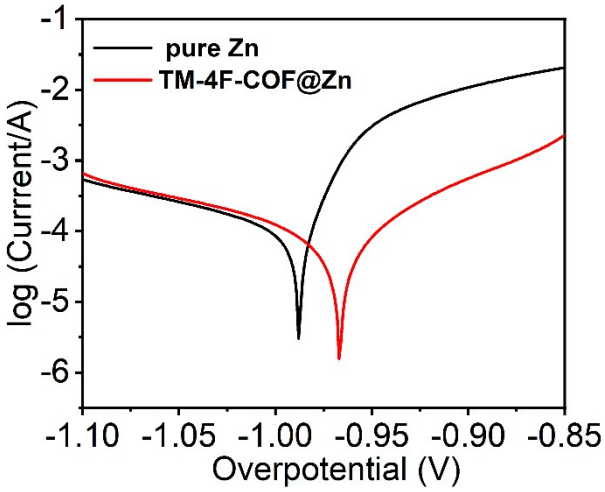

Figure S21. The potentiodynamic polarization curves of pure Zn and TM-4F-COF@Zn in 2 M $ZnSO_4$.

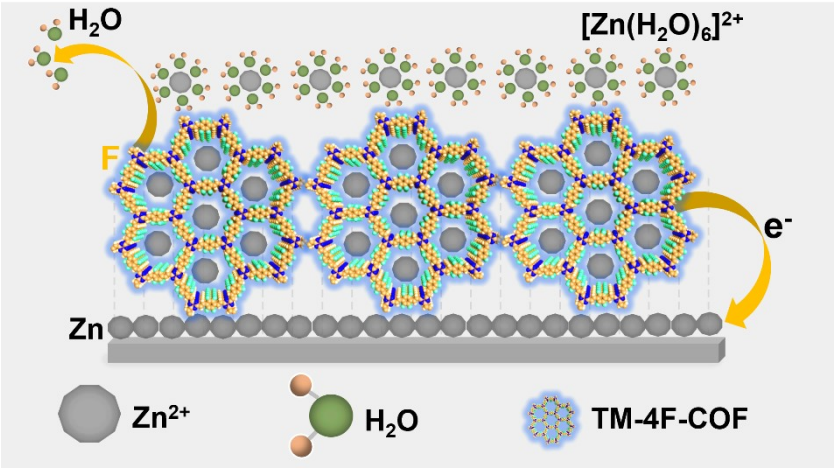

Figure S22. The performance improvement mechanism scheme for TM-4F-COF@Zn.

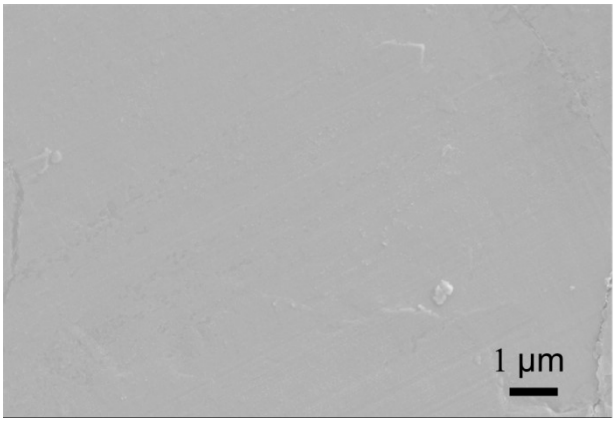

Figure S23. The SEM image of initial Zn foil.

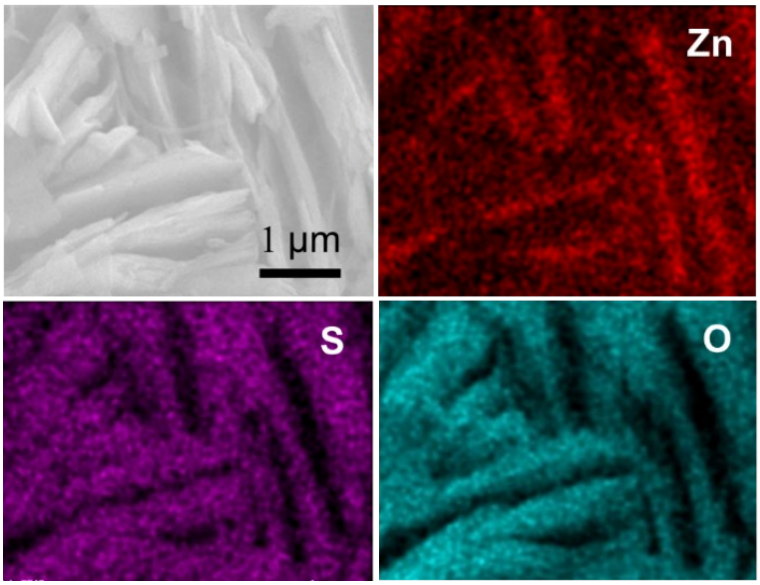

Figure S24. The EDS mapping of pure Zn anode after 50th Zn plating/stripping.

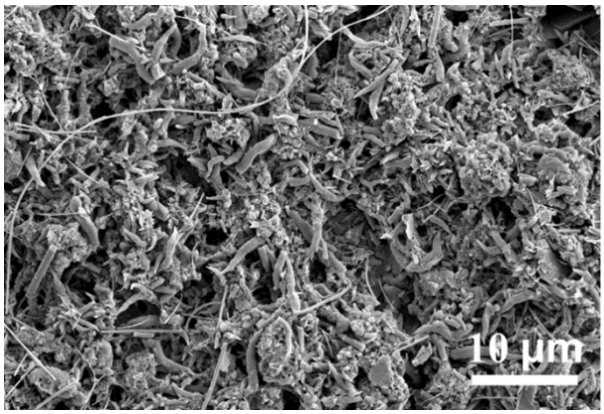

Figure S25. The surface SEM image of TM-TA-COF @Zn after 50th Zn plating/stripping.

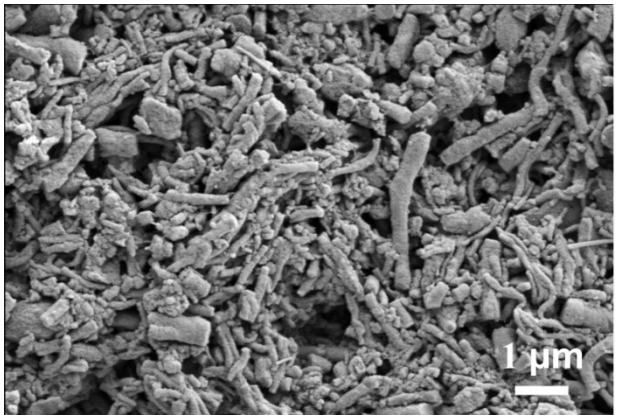

Figure S26. The surface SEM image of TM-4F-COF @Zn after 50th Zn plating/stripping.

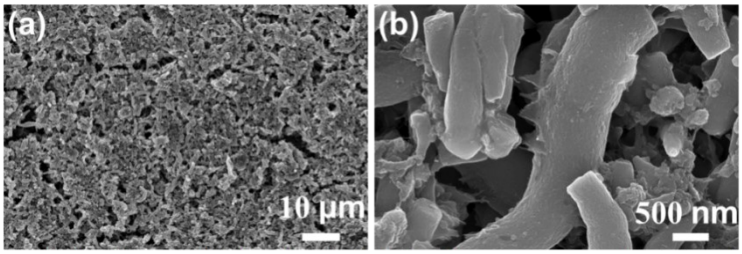

Figure S27. The low-magnification (a) and high-magnification (b) images of initial TM-TA-COF@Zn electrode.

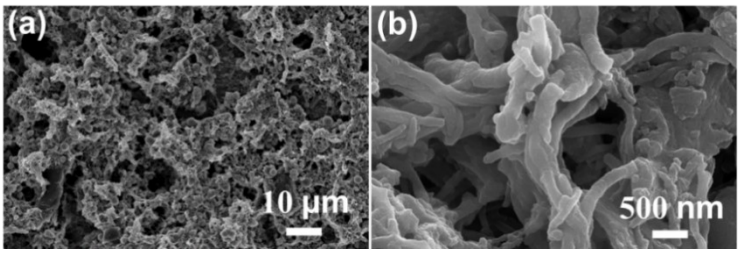

Figure S28. The low-magnification (a) and high-magnification (b) images of initial TM-4F-COF@Zn.

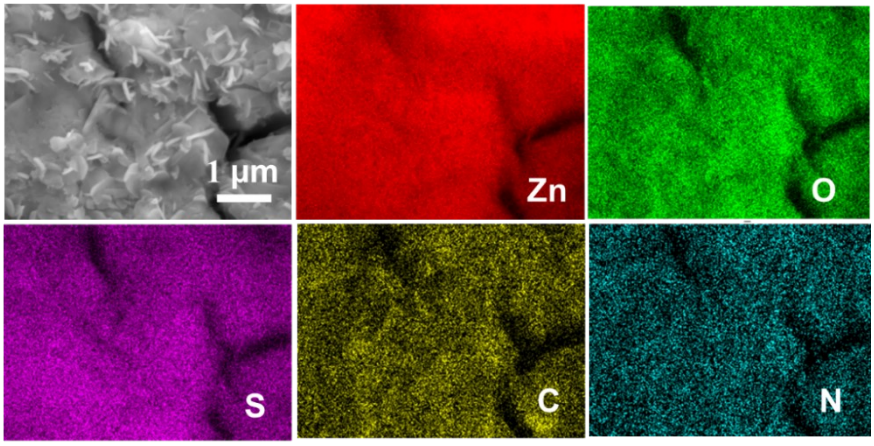

Figure S29. The image and EDS mapping of Zn deposits of TM-TA-COF@Zn after 50th plating/stripping.

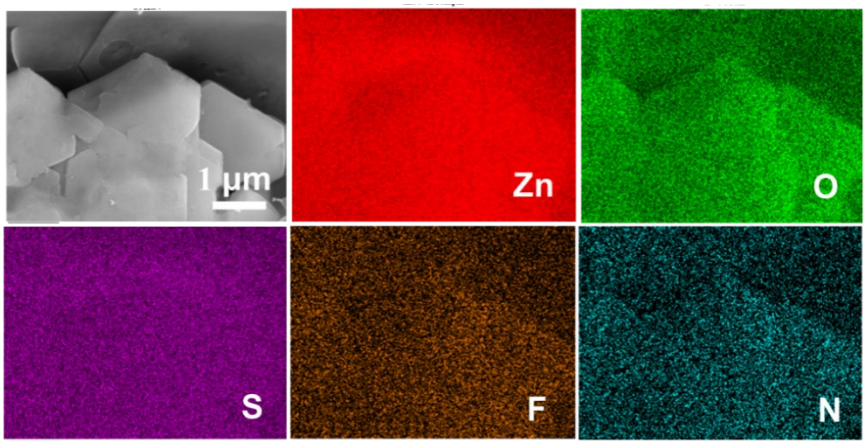

Figure S30. The image and EDS mapping of Zn deposits of TM-4F-COF@Zn after 50th plating/stripping.

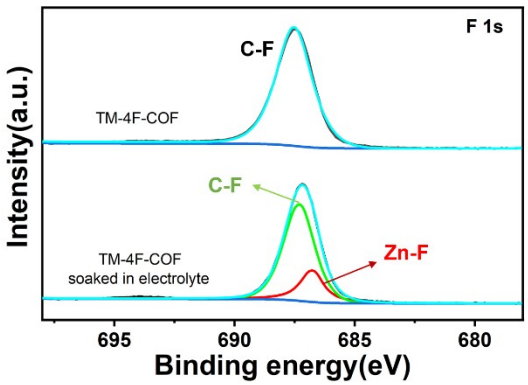

Figure S31. The F 1s high resolution XPS spectra of TM-4F-COF sample before and after soaked in 2M $ZnSO_4$ electrolyte for 3 days.

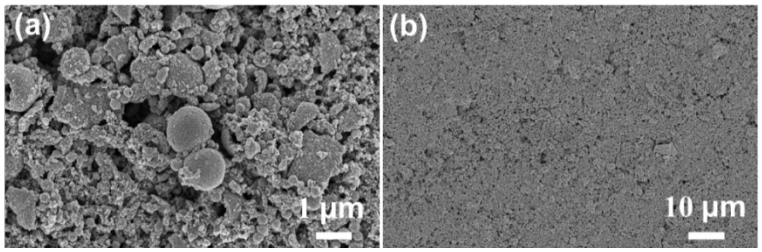

Figure S32. SEM images of as-prepared V_2O_5 electrode sheet.

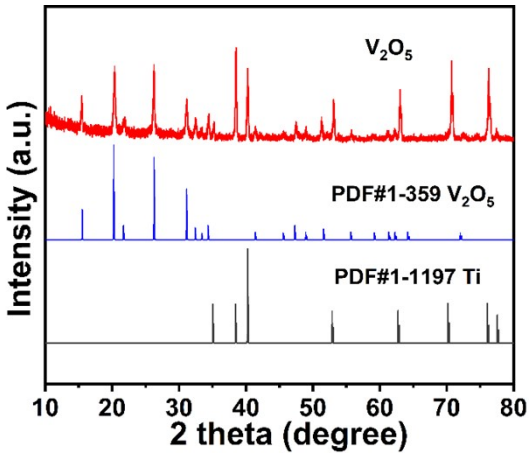

Figure S33. XRD spectrum of as-prepared V_2O_5 electrode sheet.

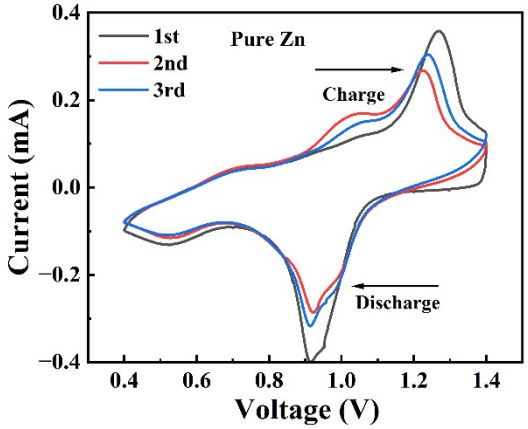

Figure S34. The CV curves of pure Zn//V_2O_5 battery.

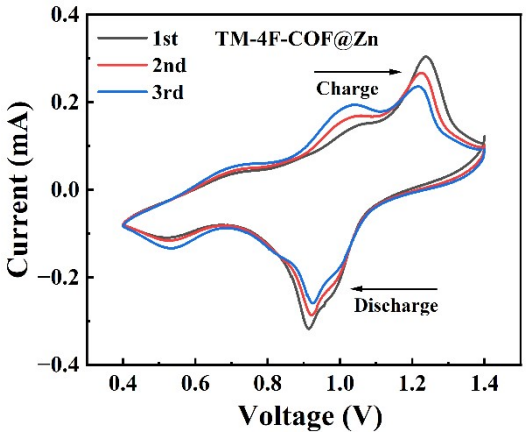

Figure S35. The CV curves of TM-TA-COF//V_2O_5 batteries.

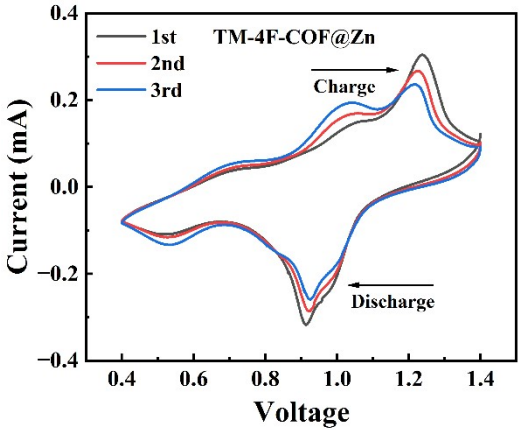

Figure S36. The CV curves of TM-4F-COF//V_2O_5 batteries.

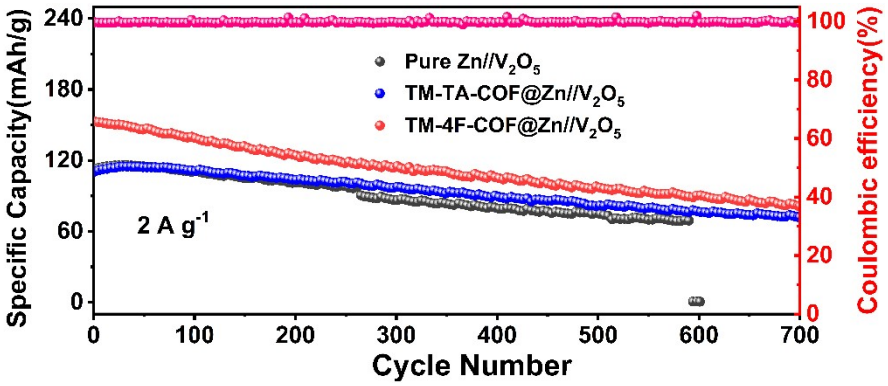

Figure S37. The cycling stability of Zn//V_2O_5 batteries.

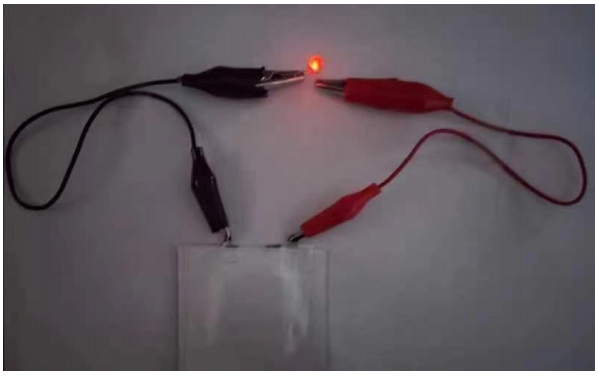

Figure S38. The lit red LED cycling stability of Zn//V_2O_5 batteries.

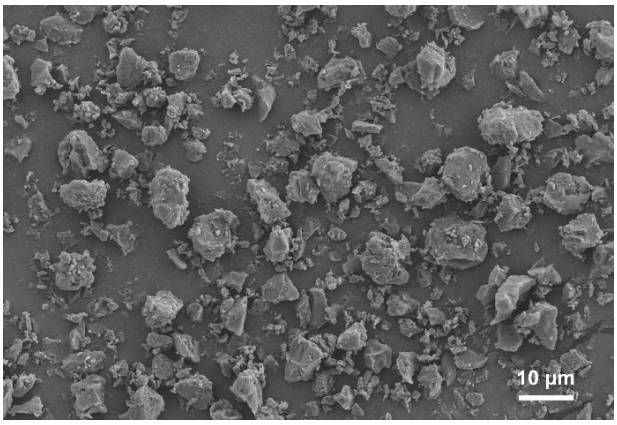

Figure S39. The SEM image of activated carbon.

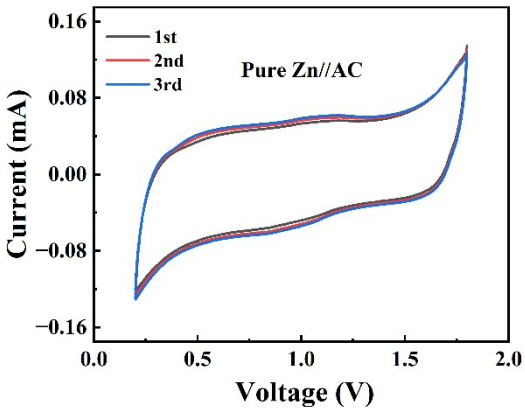

Figure 40. The CV curves of pure Zn//AC capacitors.

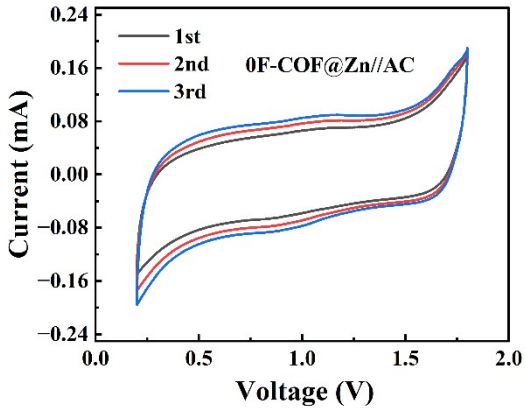

Figure S41. The CV curves of pure TM-TA-COF@Zn//AC capacitors.

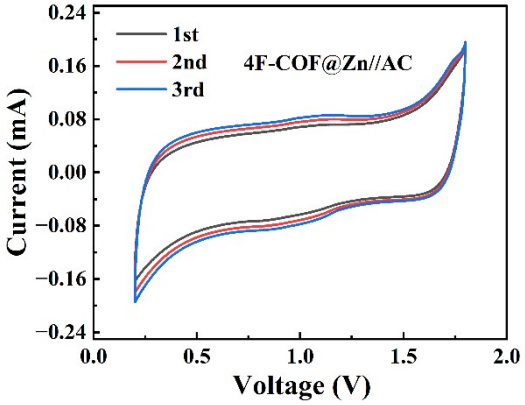

Figure S42. The CV curves of pure TM-4F-COF@Zn//AC capacitors.

Table S1. Elemental analysis data of TM-TA-COF and TM-4F-COF.

Samples		C%	H%	N%
TM-TA-COF	Calcd.	80	4.44	15.56
	Found	78.63	4.12	14.86
TM-4F-COF	Calcd.	57.44	1.6	11.17
	Found	56.76	1.03	11.12

Supporting References

[1] J. Newman, K.E. Thomas, H. Hafezi, D.R. Wheeler, *J. Power Sources* **2003**, *119–121*, 838.

[2] G. Kresse, J. Furthmüller, *Phys. Rev. B*. **1996**, *54*, 11169.

[3] J.P. Perdew, K. Burke, M. Ernzerhof, *Phys. Rev. Lett*. **1996**, *77*, 3865.

[4] G. Kresse, D. Joubert, *Phys. Rev. B*. **1999**, *59*, 1758.

[5] P.E. Blöchl, *Phys. Rev. B*. **1994**, *50*, 17953.

[6] S. Grimme, J. Antony, S. Ehrlich, H. Krieg, *J. Chem. Phys*. **2010**, *132*, 154104.

[7] G. Kresse, J. Furthmüller, *Comput. Mater. Sci*. **1996**, *6*, 15–50.